Shared human-robot proportional control of a dexterous myoelectric prosthesis

Katie Z. Zhuang, Nicolas Sommer*, Vincent Mendez*, Saurav Aryan*, Emanuele Formento, Edoardo D'Anna, Fiorenzo Artoni, Francesco Petrini, Giuseppe Granata, Giovanni Cannaviello, Wassim Raffoul, Aude Billard#, and Silvestro Micera#

(* Equal contribution as junior authors, # Equal contribution as senior authors)

Myoelectric prostheses allow users to recover lost functionality by controlling a robotic device with their remaining muscle activity. Such commercial devices can give users a high level of autonomy, but still do not approach the dexterity of the intact human hand. We present here a method to control a robotic hand, shared between user intention and robotic automation. The algorithm allows user-controlled movements when high dexterity is desired, but also assisted grasping when robustness is paramount. This combination of features is currently lacking in commercial prostheses and can greatly improve prosthesis usability. First, we design and test a myoelectric proportional controller that can predict multiple joint angles simultaneously and with high accuracy. We then implement online control with both able-bodied and amputee subjects. Finally, we present a shared control scheme in which robotic automation aids in object grasping by maximizing contact area between hand and object, greatly increasing grasp success and object hold times in both a virtual and a physical environment. Our results present a viable method of prosthesis control implemented in real time, for reliable articulation of multiple simultaneous degrees of freedom.

In the United States alone, about 1.6 million people live with an amputation, 541,000 of which affect the upper limbs[1]. This condition diminishes quality of life, mobility and independence, while also imparting a social stigma[2]. Upper limb prostheses controlled using surface electromyographic (sEMG) signals attempt to restore hand and arm functionality by using the amputee's remaining muscle activity to control movements of a prosthetic device. However, the capabilities of current commercial prostheses are still grossly inferior compared to the dexterity of the human hand. Commercial devices usually use a two-recording-channel system to control a single degree of freedom (DoF), i.e. one sEMG channel for flexion and one for extension[3]. While intuitive, the system provides little dexterity. Patients abandon myoelectric prostheses at high rates, in part because they feel that the level of control is insufficient to merit the price and complexity of these devices[4–6]In recent years, various research groups have made significant advances in myoelectric prosthesis control in laboratory and prototype environments. Many groups have demonstrated great success in grasp classification, which is a common approach for prosthesis control, but limits the user to a library of trained hand postures[7–10]. However a few groups have now attempted to decode single finger movements[11–13]. Despite high decoding accuracy, these studies showed results mainly from able-bodied subjects performing offline tests. With cited decoding performances of upwards of 90-95% for each method, we see a clear dichotomy between laboratory experiments and clinical viability, a point that is addressed by Jiang et al[14].

The idea of "shared control", that is, automation of some portion of the motor command, is already a topic of interest within the field of robotics and neuroengineering[15–18]. Indeed, shared control approach can play a key role in robotic applications involving human-robot interfacing such as prosthetic body parts. The limited sensory-motor control abilities in this case make the subjects

unable to conform their fingers to the shape of the object. This in turn inhibits their ability to secure and adapt their grasp according to the requirement of the task. Shared control can fill this void by stabilizing the grasp, making fine adjustments to the fingers by processing information from the tactile sensors placed on prosthetic hand's fingers. More generally speaking, shared control strategies aim to bridge the gap between human's intentions and efficient execution of the intended task by using information from the sensors.

Even if potentially useful, shared control has not yet become prevalent in the area of peripheral nerve interfaces. Došen et al. propose a camera-based approach[19]while Light et al. proposes 1-DoF control with automated grip force adjustment[20]. Other methods of automation include automated hand-closing in response to slippage[21] and underactuated systems in which spring-like mechanisms mediate grasp force[22]. The only commercial application of shared-control methods to date is the Ottobock Sensorhand Speed which automatically increases thumb flexion during grasping in response to slippage[18]. However, it is only capable of binary action choices or 1-DoF proportional velocity control.

The control method presented here attempts to implement a shared-control strategy with a highly-dexterous hand prosthesis by taking advantage of state-of-the art myoelectric decoding as well as an algorithmic controller for grasp optimization. We first propose a kinematic proportional decoder using a multilayer perceptron (MLP), which allows users to simultaneously and continuously control each finger individually. In addition, we propose to integrate and use a shared-control scheme in which a robotic controller aids in stable grasping by maximizing the area of contact between a prosthetic hand and an object[23]. The idea behind this scheme is to make object grasping more robust (avoiding accidental drops) while allowing the user to maintain full autonomy over grasping or releasing, grasp preshaping, and non-grasp-related motions. In this way, we achieve both highly dexterous user control when precise positioning is valuable, and partially automated grasp attainment when object droppage avoidance desirable.

Results

We performed three sets of experiments in which we decoded hand movements of subjects using sEMG signals recorded from their forearms. We recruited three subjects with hand/transradial amputations (subjects A1, A2 and A3) and eight able-bodied subjects (subjects B1, B2, B3, B4, S1, S2, S3, S4) for the study. In the first set of experiments, able and amputee subjects performed online control of a virtual prosthetic hand. In the second set of experiments, the same subjects used a virtual hand to grasp and release virtual objects according to visual cues in two conditions: with or without robotic assistance. In the third set of experiments, four able-bodied subjects controlled a physical robotic arm and hand to perform functional object manipulation tasks.

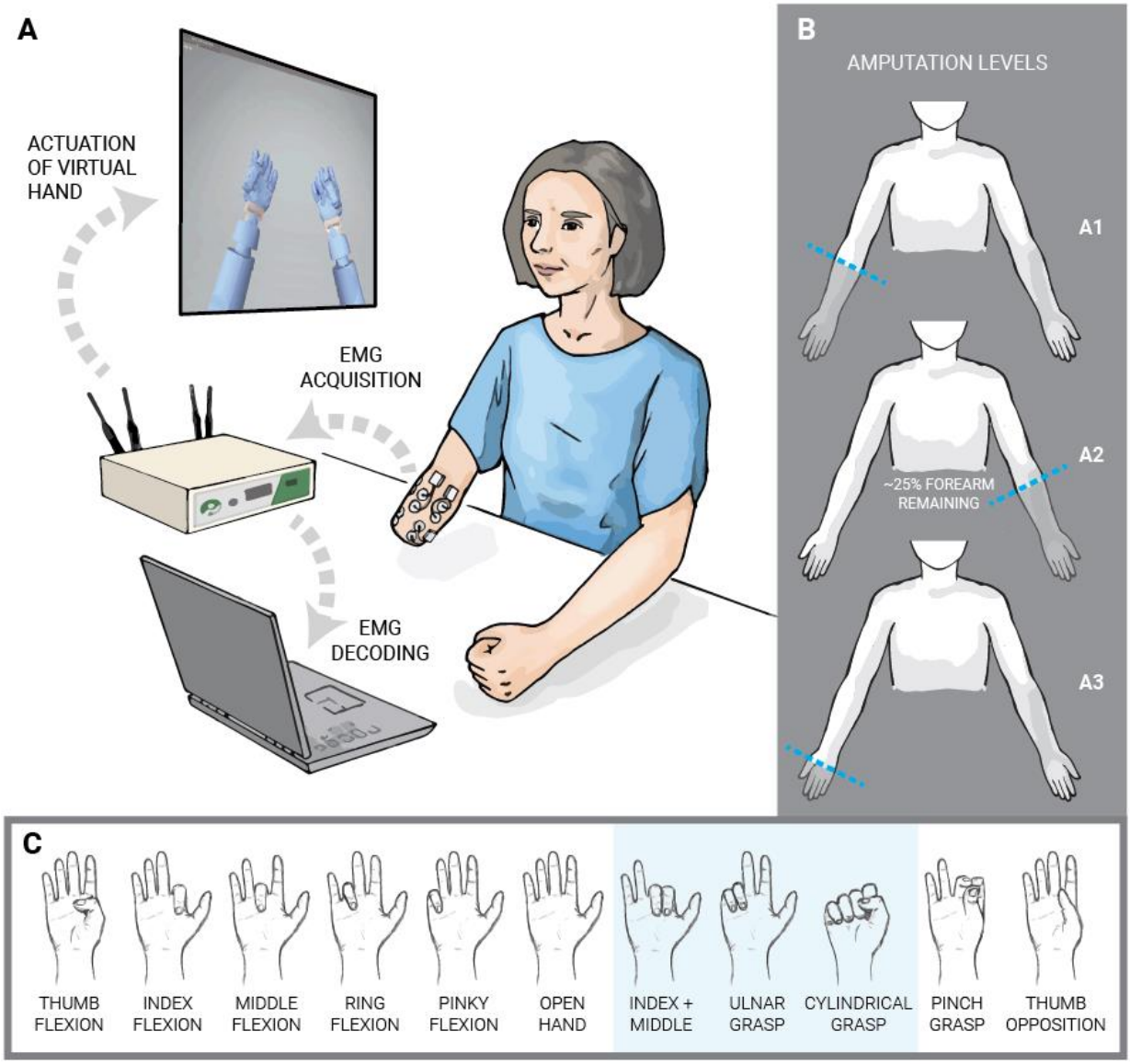

Figure 1. Experimental Setup and Subjects. **a,** In online experiments, four able-bodied subjects and three amputee subjects controlled a virtual robotic hand using their surface EMG signals. The signals were decoded with a multilayer perceptron to obtain predictions of single-digit joint angles. **b,** The three amputee subjects had varying levels of amputation, shown here. **c,** Movements we tested consisted of both single-digit and multi-digit movements. All subjects performed all movements except Subject A2 who did not perform index and middle finger flexion/extensions independently.

Experiment 1 (Online Kinematic Decoding). Three amputee subjects (A1, A2 and A3 in Figure 1b) and four able subjects (B1, B2, B3, and B4) performed online control of a virtual prosthetic hand with sEMG decoding. To train the MLP, subjects were asked to mimic the movements of the virtual hand while sEMGs were recorded. We decoded flexion and extension of each digit as well as thumb opposition and reposition. This gave DoFs per subject for all subjects except subject A2 who moved the index and middle fingers concurrently (Figure 1c). The average per-session correlation for all subjects and all sessions was 0.52 and the peak-to-peak normalized mean square error[24] (nMSE) was 15.7%. For all subjects, the MLP successfully predicts the flexion and extension of each finger, both individually and simultaneously with flexion of other digits. We summarize performance in Supplementary Table 1 for all subjects and sessions.

In order to further analyze the ability of the decoder to predict the desired joint angles and to compare these predictions against chance, we computed the percentage of time of correctly predicted joint angles for each subject (Figure 2a). As a control for this assessment, we selected random angles

from the training set range and computed prediction accuracy using the random angle as the instructed one (white sections). This way, we were able to simulate chance accuracy of the MLP predictions. We find that in every degree of freedom for Subject A3, the MLP is able to decode significantly higher than chance (Wilcoxon two-sided signed rank test, $p<0.01$). The same analysis was performed for all subjects individually with similar results (Supplementary Figure 2) using a non-parametric test due to non-normal data (Komolgorov-Smirnoff test). We then performed this analysis for all subjects while pooling all of the degrees of freedom to obtain an overall measure of decoding performance (Figure 2b).

To analyze any patterns in prediction error, we calculated a “confusion matrix” for each degree of freedom (Figure 2c). Here, we enforced a threshold (mean prediction angle) to separate joint predictions into either flexion or extension. We also mapped the instructed joint angles into flexion or extension using mean instructed angle for thresholding. Plotting instructed activation on the x-axis and performed action on the y-axis, we color map excessive action (false positive) to orange intensity and lack of action (false negative) to blue intensity. We observed that Subject A3 has trouble controlling thumb flexion; it is excessively flexed during the actions of other fingers. Similarly, Subject A2, who has extensive median nerve damage, has difficulty controlling the thumb, index and middle fingers movements.

These thresholded decoding accuracies are within a similar range as the ones obtained in online classification of finger flexion and extension cited by Cipriani et al. (79% average accuracy for amputees cited vs. our average of 89.5% for a similar number of classes: 7 classes cited vs. our 6 effective classes which are simultaneously considered).[12]

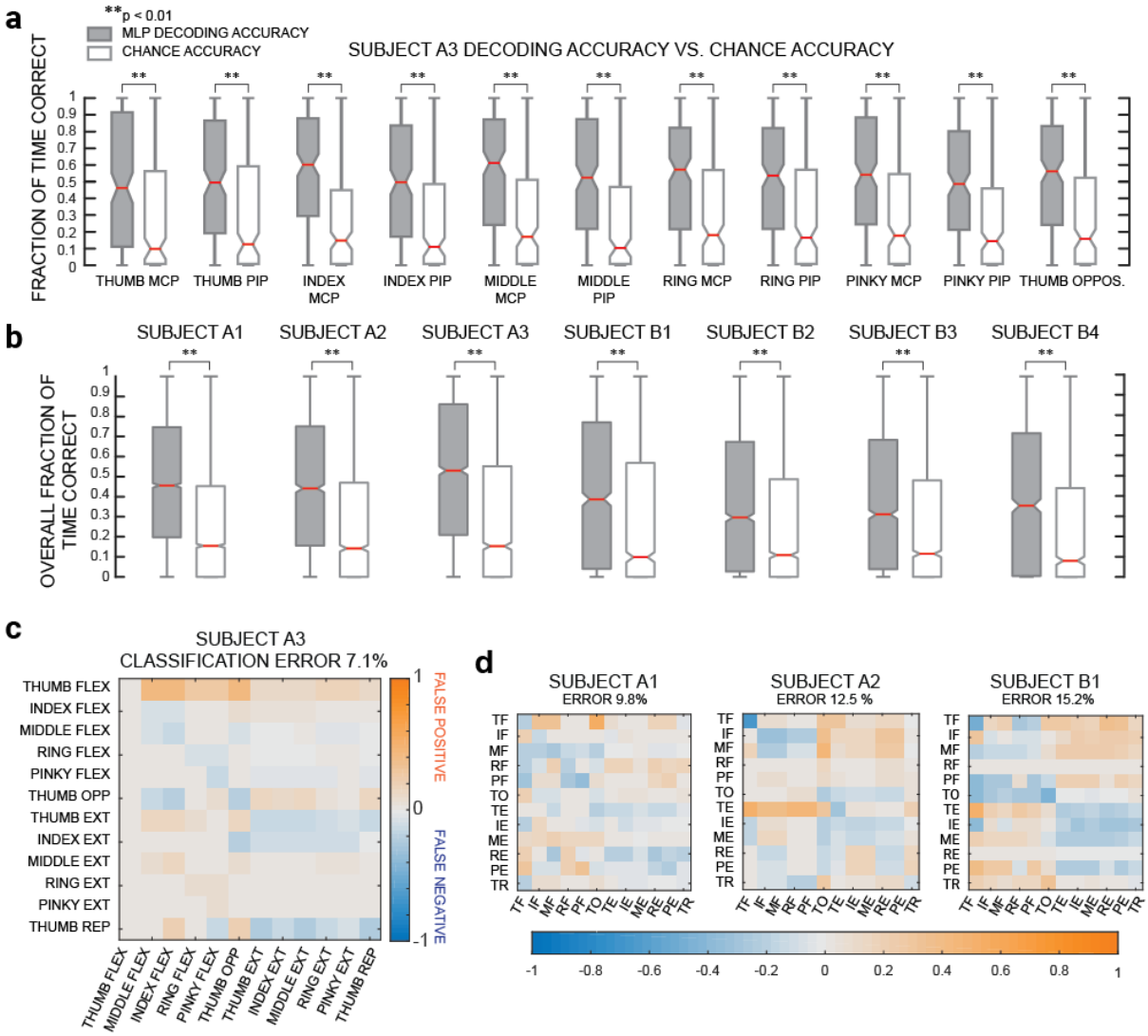

Figure 2. Analysis of online prediction performance of the MLP. **a,** Prediction accuracy of the MLP compared to chance accuracy. Gray boxplots indicate the fraction of time per trial that each predicted DoF is within 15 degrees of the instructed angle. White boxplots indicate the fraction of time per trial that a random angle (within the set of trained angles) is within 15 degrees of the instructed angle. Each degree of freedom was predicted higher than chance level ($p<0.01$ Wilcoxon two-sided signed rank test). All box plots in this manuscript include a median center line (red), box edges at 25th and 75th percentiles, notches calculated based on interquartile range $\pm\frac{1.57*IQR}{\sqrt{n}}$ **b,** Overall decoding accuracy versus chance for all subjects. Statistical significance is calculated with the Wilcoxon two-sided signed rank test. **c,** Confusion matrix of each digit's degrees of freedom for one subject. Blue pixels indicate lack of specified movement when instructed (false negatives) while more orange pixels indicate undesired movements (false positives). Overall error is calculated as well as error along the diagonal of the matrix (whether the instructed motion was performed accurately). **d,** Confusion matrices for three other subjects.

This experiment demonstrates our ability to decode individual finger movements proportionally for multiple simultaneous DoFs and in real time using noninvasive sEMG signals. Performance results are not only above chance level, but robust for all tested movements for both able-bodied subjects as well as amputee subjects.

Experiment 2 (Shared Control using the virtual environment). In this set of experiments, the user attempted to grasp, hold and then release virtual objects by controlling a sensorized virtual robotic hand implemented in Gazebo and rviz, a ROS package (Figure 3a). The same subjects from Experiment 1 performed this experiment with the exception of subject B1. In addition to the MLP decoding, we tested two conditions: one *with* shared control for partial grasp automation (shared control) and one *without* (MLP only). During the shared control condition, the virtual hand would

automatically attempt to maximize contact between the hand and a grasped object by increasing flexion of a finger as soon as a single phalanx touches an object. If, however, the total joint angle difference between MLP predictions and shared control targets of a single digit would differ by more than 50 degrees, the controller would use torque control to achieve MLP-decoded joint angles for that digit (Figure 3b). This threshold was chosen empirically from preliminary testing. In the future, we will strive to make the transition gradual instead using a threshold. The action of the algorithm is shown in Figure 3c under the conditions of pre-contact (MLP joint targets), initial contact (shared control targets in red) and achievement of full contact (in green). Figure 4d shows an example of single-digit flexion and extension with or without shared control for Subject B4 grasping the thin rectangular bar. We see that when shared control is implemented, digits that make initial contact with an object are better able to achieve more contacts and maintain them. The higher number of contacts achieved with shared control reflects this advantage (top row). However, the user is still able to release the object when it is desired (movement instructions at bottom).

In Figures 3e, 4a we show the percentage of trials in which a full grasp is achieved per subject across all sessions with either shared control or only MLP predictions. Full grasp is defined as attaining all possible contacts between the hand and a particular object (see Methods). In the shared control condition, subjects are able to achieve considerably more successful grasp trials for all objects. For

each object and for each subject, we also show percentage change in fraction of successful grasp trials between the MLP-only and shared control conditions (Figure 4b).

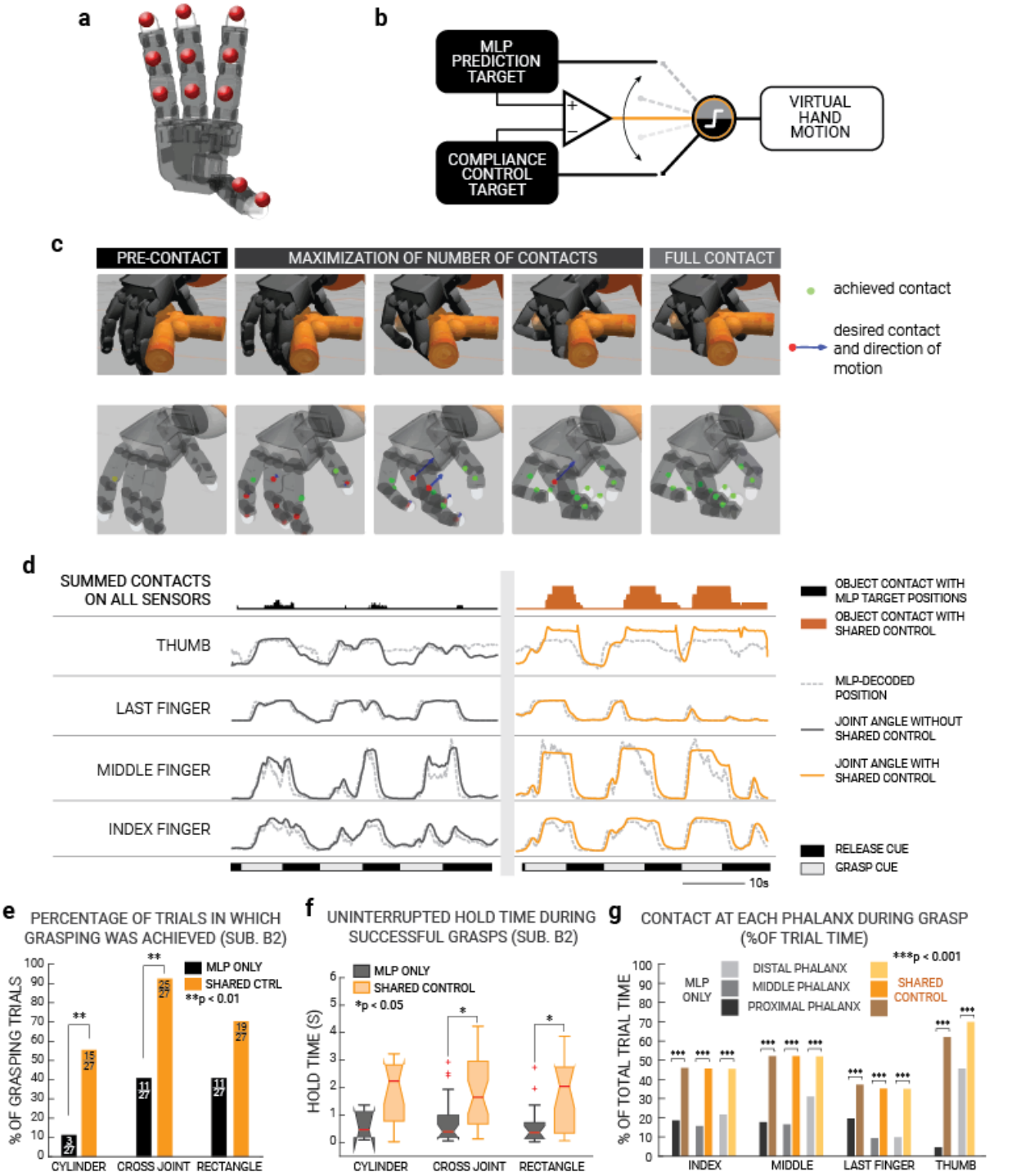

Figure 3. Shared control in virtual environment, setup and results. **a**, Simulator of Allegro Hand **b**, Shared control scheme. Both the MLP decoder and shared controller run simultaneously and the MLP-decoded joint targets prevail before contact. During object contact, the shared control joint targets prevail unless the difference between MLP-only and shared control is above a 50-degree threshold. **c**, Action of the active compliant contact controller. When one contact on a digit touches the object, the direction of motion is computed to bring other contacts of the digit towards the object. Figure adapted from Sommer and Billard et al.[23] **d**, Example traces of shared control (Subject B4). Top row shows total of pressure detected without (left) and with (right) shared control. Traces show the joint angle for each DoF. Dotted lines indicate the MLP prediction while solid traces indicate the actual position of the virtual robotic hand. Bottom row indicates the cues to grasp or release. **e**, Percentage of trials during which desired contacts are achieved for the three objects by Subject B5 over 3 sessions. (p-values from Fisher's two-tailed exact test). Number of successful trials versus total trials are indicated on each bar. **f,** Duration of hold time for each object out of seven seconds (p-values from Wilcoxon two-sided signed-rank test). **g**, Percentage of grasping trial time during which contacts were touching the objects (p-values from Fisher's two-tailed exact test). Contacts on different phalanges are indicated with different color shades, raw numbers for calculation included in Supplementary Table 1.

We also see a difference in grasping performance between objects grasped which is subject-dependent. For example, Subject A2 benefitted the most from shared control for the rectangular bar. This result is consistent with the finding that the same subject has particular difficulty in sustaining muscle activation associated with the thumb, index and middle fingers due to median nerve damage.

In addition to the attainment of grasp, we also assessed how long the subjects were able to maintain holds. Figure 3f, 4c shows the distribution of hold times per object and per subject with or without shared control. We define hold time as the length of continuous time during which the subject could maintain required contacts between the virtual hand and object without any contacts being broken[25].Due to the visual cue, a small percentage of non-hold time is likely due to subject reaction time. For all objects and subjects, hold times are greater with the shared control condition than only MLP, with the exception of the cylinder for subject B2.This may be due to the low number of trials subject B2 performed in comparison to Subjects A1-3. .

Finally, we assess the percentage of time that each single sensor contacted the objects to analyze which contacts subjects found more difficult to maintain. For all objects, all subjects were able to maintain longer contacts with all parts of the digits with shared control than with only MLP predictions. Importantly, all subjects were capable of releasing the objects once grasped by relaxing their grasp (Fig. 4d, 6b).

Taken together, these results show that the shared controller aids grasping in multiple ways, namely facilitating longer, more successful grasps and avoiding accidental drops.

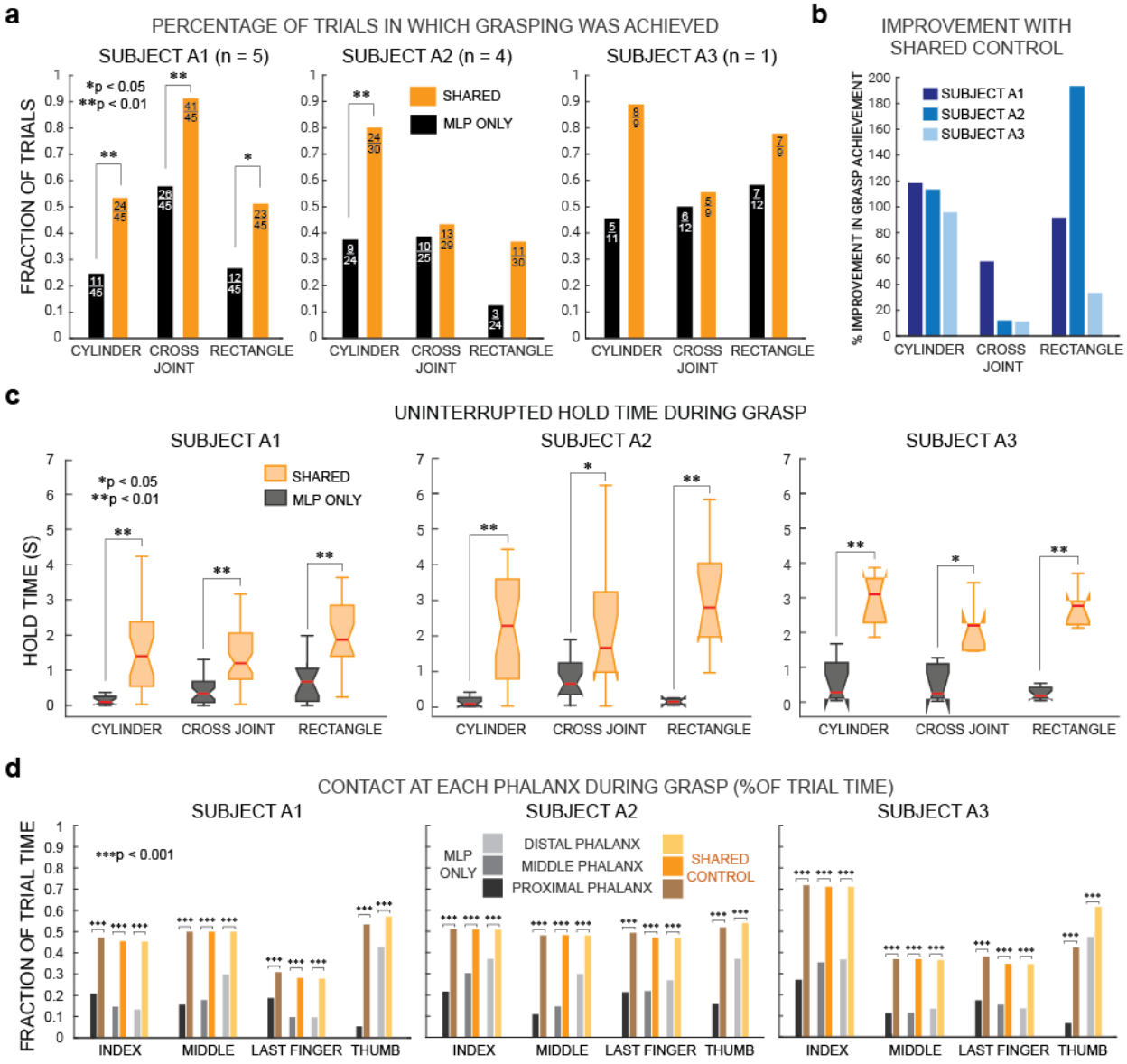

Figure 4. Shared Control results in virtual environment cont'd. **a,** Comparison of fraction of successful grasping trials with (orange) or without (black) shared controller aid for three amputee subjects and all three object types. Data are shown for all sessions of each subject (# of sessions indicated in title). Statistical p-values are computed using Fisher's two-tailed exact test. Number of successful trials versus total trials are indicated on each bar. **b,** Percentage improvement in fraction of correct trials for the three subjects split by object type. Each color indicates a different subject. **c,** Duration of hold time for each object with or without shared control for the three subjects (p-values by Wilcoxon two-sided signed-rank test). Maximum instructed hold time was seven seconds. **d,** Percentage of grasping trial time during which each single contact on each digit made contact with the objects with or without shared control for the three subjects (p-values by Fisher's two-tailed Exact Test). Each plot is for a different subject with the shaded bars indicating contact placement. Lighter color shades indicate more proximal phalanges on the same digit. Data are aggregated over all trials and sessions for a single subject, raw numbers for calculation included in Supplementary Table 2.

Experiment 3 (Shared Control in a physical environment).

This experiment was divided into two sub-experiments. In the first sub-experiment, the subjects performed a variant of the box and block test[26] through teleoperation of a physical robotic hand and arm. The goal was to grasp and move an object (a bottle, half-filled of water) placed on a hard case to another one placed approximately 30cm away. Object droppage was considered a failed trial. The subjects controlled the robotic arm via an optical motion capture system. A robotic hand (the physical analog of the virtual one described in Experiment 2) was mounted onto the robotic arm and controlled with either MLP only or shared control. Four able-bodied subjects participated in this experiment (S1, S2, S3 and S4). After a training phase to train the MLP decoders, the subjects were required to

perform 20 trials of the functional task under in each condition (randomized MLP only and shared control) for a total of 40 trials.

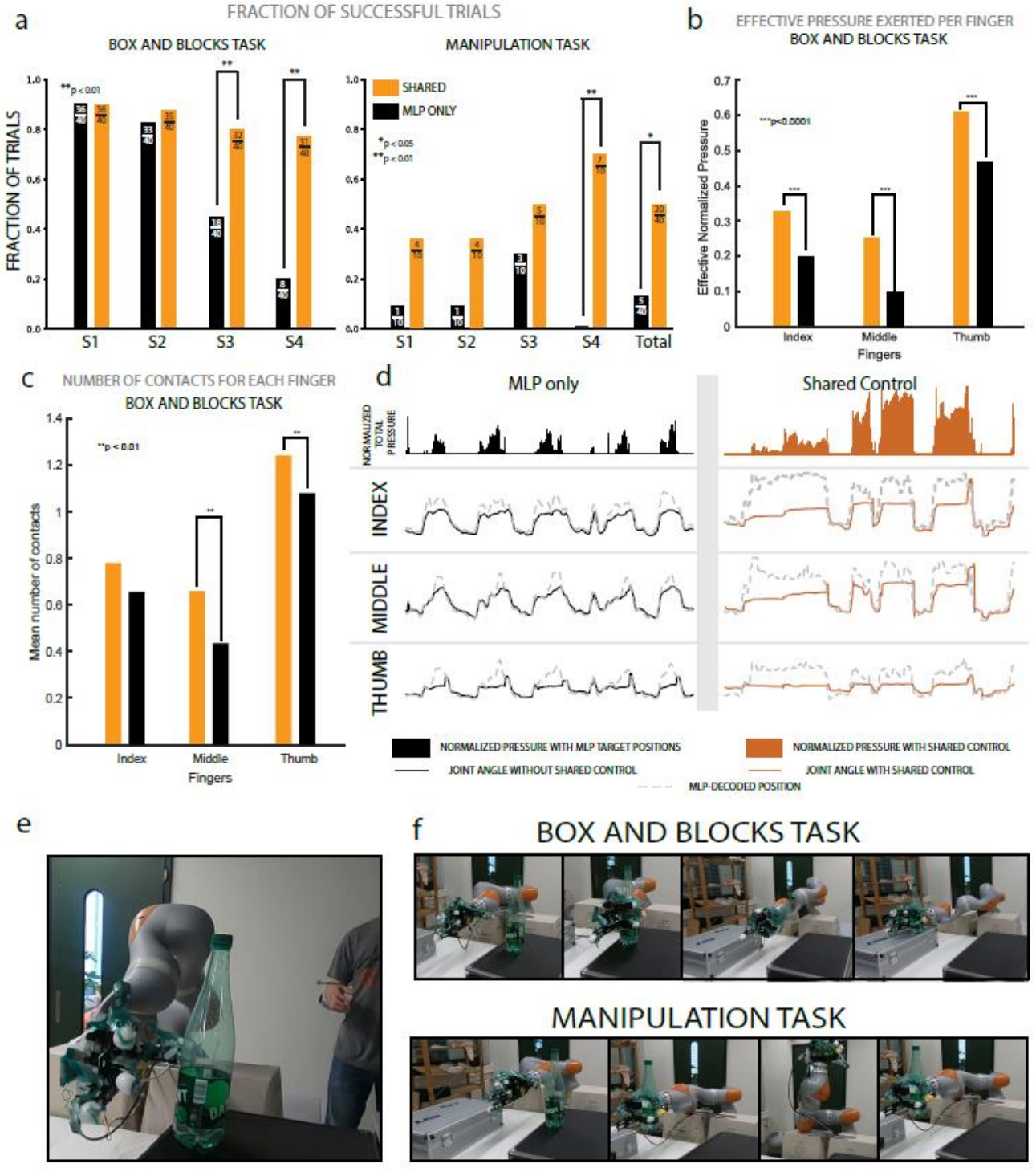

Figure 5. Shared control in physical environment, setup and results. **a,** Comparison of fraction of successful trials for the box and blocks task and the manipulation task with shared control (orange) and without (black). Data are shown for all sessions of each subject. Number of successful trials versus total trials are indicated on each bar when not zero. For the manipulation task (right panel), the total number of successful trials in each condition was summed over all the subjects. Fisher's two-tailed exact test was used to compute statistical p-values for individual subjects, Wilcoxon rank-sum test was used for total values. **b**, Effective normalized pressure on each finger comparing the trials with and without shared control. The p-values indicated were computed using Wilcoxon's rank-sum test. **c**, Number of contacts detected by pressure sensors on each finger, averaged over time of each trial. The bars indicate the mean of each trial's average number of contacts. The p-value is computed using Wilcoxon's rank-sum test to compare trials of all subjects with and without shared

control. **d**, Time series plots of total pressure, MLP decoded joint positions (dotted) and corresponding actual joint positions of the allegro hand (solid) over few sample grasping trials. The joints on each finger were summed over phalanges. Total pressure was computed by summing over all phalanges after normalization. **e,** Picture of the setup comprising the robotic arm and hand with a subject wearing the EMG acquisition system. **f,** Snapshots of completion of box and blocks task (top) and manipulation task (bottom). For full video see supplementary video 3. One trial of each condition (with and without shared-control) can be seen in supplementary video 4.

Results are shown in Figure 5a (left panel). S3 and S4 performed significantly better with shared control than without whereas S1 and S2 were highly successful at the task in both conditions.

To evaluate whether the shared control improves grasp quality, we defined two metrics based on the pressure sensor data: average number of contacts and the "effective normalized pressure" (see Methods). The results shown in figures 5b and 5c indicate better performance with shared control in terms of both of the two metrics. The p-values, computed using Wilcoxon's rank-sum test over all trials by all subjects, show statistical significance in case of effective normal pressure ($p< 0.0001$). The same test performed on average number of contacts was not significant for the index finger ($p=0.07$) but showed statistical significance for the other two fingers ($p< 0.05$).

As shared control was notably advantageous for the subject S3, we compared the timeseries plots of a few trials from the subject's box and block tasks (Figure 5d). In open position (close to zero), the actual position (solid line) closely follows the MLP prediction (dotted line) for each finger. However, the subject cannot close the fingers enough to grasp, leading to insufficient total pressure. With the shared control, the grasps are tightened to achieve the desired pressure. In case of the subjects who performed equally well with and without shared control (S1, S2) the MLP prediction by itself was high enough during grasping to achieve a tight grip and high pressure.

The second sub-experiment used the same training protocol as first, with a slight variation in the behavioral task. The task here consisted of grasping the bottle from the table, bringing it to mouth, tilting it to mimic drinking and then returning the bottle back to a steady position (a few centimeters above the table). Subjects were given less than 10 seconds to complete the movement and then hold the bottle in steady position for at least 10 seconds. The rotation of partially filled bottle leads to the shifting of its moment of inertia due to flow of the water, resulting in a perturbation. Additionally, bottle's conical shape and smooth surface further adds to sliding of the bottle. Thus, this sub-task can evaluate the potential of shared control in stabilizing the grasp under object's perturbations, slippery surface and non-uniform shape of object. S1, S2 and S3 performed better with shared control but not significantly (S1 and S3: $p=0.3$, S2: $p=0.65$) while S4 showed statistically significant improvement (Figure 5a right). This is likely due to the limited number of trials. Moreover, S4 was completely unsuccessful at completing the task without shared control but performed relatively well with shared control ($p < 0.01$). The overall advantage of using the shared control becomes evident when we pool together all the subjects (see last histograms in Figure 5b).

Discussion

Here we show that we are able to decode single finger kinematics from surface EMGs of both able and amputee subjects. The decoding approach was accurate for both single-finger movements and coordinated, simultaneously activated grasping motions. We also show that decoding is fast enough for real-time applications, with an update rate of 33 Hz. To the best of our knowledge, the work presented here is the first demonstration of a real-time proportional decoder for individual fingers tested with amputee subjects.

One reason commercial prostheses prefer to implement classifier-based decoders instead of proportional ones is the robustness of classifiers in remaining in a particular posture. For grasping, this type of control is ideal to prevent accidental dropping but sacrifices user agency by restricting the number of possible hand postures. Our implementation of shared control allows for both user agency

and grasping robustness. In free space, the user has full control over hand movements, which also allows for volitional pre-shaping for grasping.

The tests performed in a physical environment allowed us to show the efficacy of shared control to the improvement of grasp especially when complex tasks are implemented (see Figure 5b). For the first simpler sub-experiment, some subjects (S1 and S2) performed the tasks equally well regardless of the use of shared control while others (S3 and S4) benefitted from shared control significantly. This was because the MLP prediction performance varies across the subjects. These results show that the use of the shared control can be particularly useful for subjects with limited EMG control ability.

Another advantage of shared control is that it requires less energy for the user to maintain a grasp[14]. Muscle fatigue is well-documented in sEMG studies[27–31] and is one hurdle for proportionally controlled prostheses. Without the presence of sensory feedback, the simplest solution for a user to be sure of sufficient force is to flex the fingers maximally throughout the duration of the grasp, which can be very fatiguing. In Figure 6b and 6c we show EMG activity of Subject B2 during grasping with shared control or with only MLP predictions. Figure 6b shows averaged EMG activity across all channels and all grasp trials of each object type in a session. As can be seen, for all objects, EMG amplitude is lower with shared control ($p<0.01$ Wilcoxon two-sided signed rank test). As a control, we also plot averaged EMG during release trials (Fig. 6b right) which reveals low EMG activity for all objects, after a short peak at the beginning of the trial during which the subject reacts to the visual cue to release. Figure 6c shows the averaged EMG for each individual channel and for each individual object averaged across trials with only MLP predictions (left) or shared control (right). We observe a clear difference in overall muscle activation. This effect on EMG activity was also confirmed during Experiment 3. Figure 6d shows averaged EMG activity across all grasps and all EMG channels for each subject. EMG activity is significantly different for subject S1 and S4 ($p<0.01$, Wilcoxon two-sided signed rank test), but not for S2 ($p=0.64$) and S3 ($p=0.61$). It is interesting to note that even two subjects performed well for the box and blocks test in both conditions (see Fig. 5a), the overall muscle activation is clearly lower during shared control than the MLP-only condition. We find the same result when we analyze each EMG channel separately (Figure 6e).

In our study, inter-subject decoding performance was highly inconsistent. For amputee subjects, many factors can contribute to this heterogeneity, including the level of amputation (Figure 1b), type of injury and time since injury. In Figure 6a we plot the correlation coefficient between the EMG channels we recorded from for each subject. We see that subjects A1 and A3 have relatively uncorrelated EMG channels whereas subject A2 has highly correlated channels. This indicates inability to activate different muscle groups independently. Functionally, this results in subject A2's inability to perform all of the single-digit movements that the other subjects were able to In addition to a lower number of DoFs independently required for subject A2 (index and middle fingers moved together), we show that shared control can be particularly effective for subjects with few independent muscle groups We emphasize this point because regardless of the type of decoding algorithm one would implement, the subjects with lower neuromuscular ability will suffer lower decoding accuracy unless they can use some kind of compensation. Such compensation can be surgical, such as in

targeted muscle innervation, behavioral, such as learning to contract in an unintuitive way, or it could be algorithmic, as we implemented.

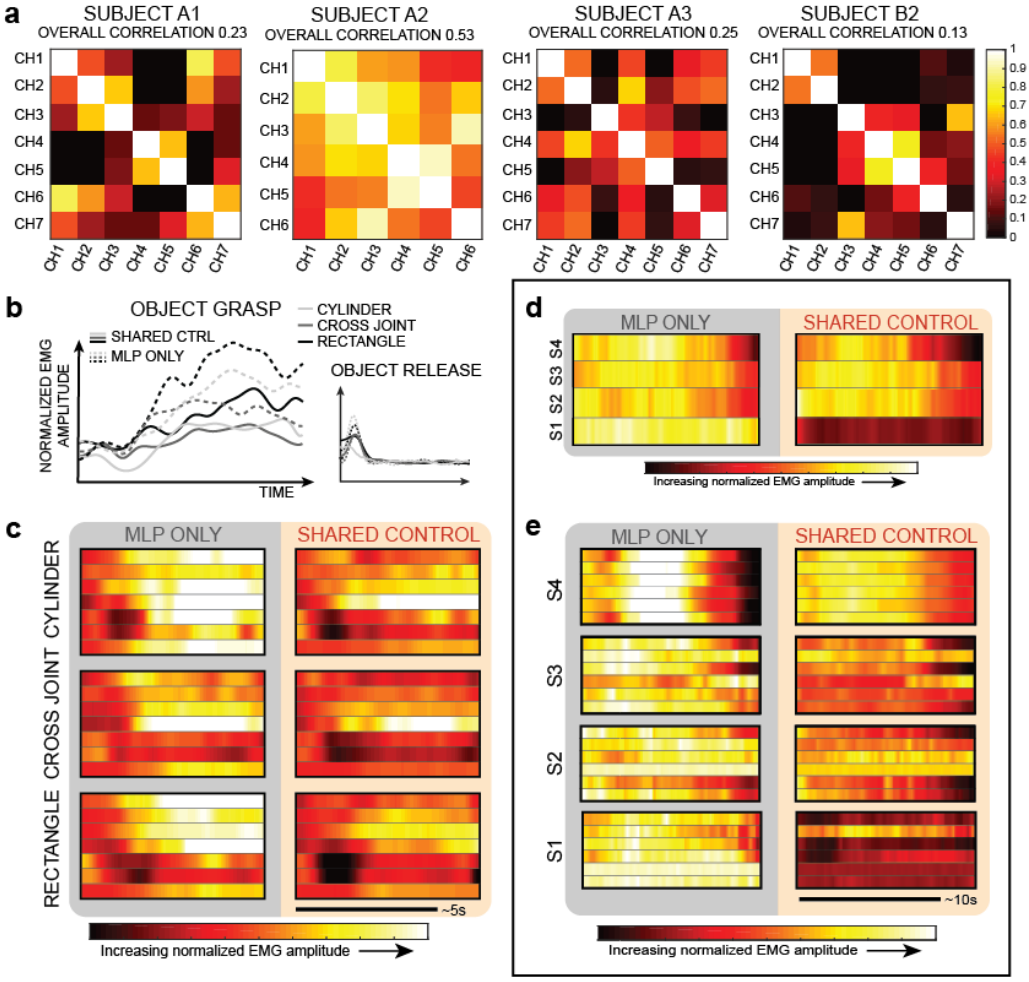

Figure 6. EMG analysis with and without shared control. **a,** Cross-correlation of EMG activity between each of the recorded channels for four subjects during a single session of MLP decoding. Darker pixels indicate lower correlation between pairs of EMG channels while brighter pixels indicate high correlation. High correlation is a proxy for muscle coactivation. **b,** Averaged sEMG amplitude during grasping trials for Subject B2 for the three objects in the virtual environment. Solid lines indicate EMG amplitude during grasp trials of shared control and dashed lines indicate average EMG amplitudes during trials with only MLP control (left). The same plot is shown for release trials: when the subject was instructed to release the object (right). **c,** Per-channel EMG activity during grasp trials of each object for Subject B2. Each row is normalized amplitude of a single EMG channel averaged over all grasping trials for a particular object. **d,** Averaged EMG activity during grasps of the physical box and block task for each subject. Activity is averaged across all grasps and all channels per subject**. e,** Per-channel EMG activity of grasps during one session of the physical box and blocks task for each Subject. Each row is normalized amplitude of a single EMG channel averaged over all trials for a particular subject.

As of now, the compliance controller implemented in our shared control has only one set target force for applying pressure on grasped objects. Future studies should include user-modulated forces, which would be greatly aided with the addition of sensory feedback.

In conclusion, we have explored sEMG-control of individual finger movements in real time with both able-bodied and amputee subjects and show the advantages of a shared-control scheme. In particular, our shared controller leverages the dexterity afforded by user control with the grasp robustness of automation, which can greatly benefit the translation of myoelectric control algorithms into commercial devices. Furthermore, we recognize that amputees and even able users are extremely varied in their ability to modulate their remaining muscle activity. Consequently, some

subjects will be less able to control as many DoFs, or as consistently, as others. Shared control can particularly help these users who are less proficient in sEMG modulation and additionally may prevent premature fatigue. Thus, control algorithms should account for user variance and partial automation is one such method that can greatly improve myoelectric prosthesis usability. In the next future, we believe that this approach could be valuable to cope also for the limitation of other human-robot interfaces such as the ones based on brain signals or body movements.

Methods

Subjects and EMG recording. Three amputee subjects were recruited for this study, two female (Subjects A2 and A3) aged 53 and 49, respectively, and one male (Subject A1) 69 years of age. Subjects A1 and A2 had proximal transradial amputations while subject A3 had a right hand amputation just distal to the wrist (Figure 1). In addition, seven able bodied subjects were recruited, all of whom were male, between 26 and 30 years of age for experiment 1 and 2. Subject B6 was left-handed and performed all experiments with the left hand. Four additional male subjects aged between 20 and 26 (S1, S2, S3, and S4) were recruited for the third experiment with the physical robot. Ethical approval was obtained by the Institutional Ethics Committees of Policlinic A. Gemelli at the Catholic University, the Italian Ministry of Health, and the cantonical ethical committee of Vaud. Informed consent was obtained from all participants in the study.

In Experiments 1 and 2, we collected data from three able-bodied subjects (subjects B2, B3, and B4) and all three amputee subjects. Subject B1 performed only Experiment 1. For the three experiments, we used the Noraxon Delsys system connected to a LabJack data acquisition card to wirelessly record from five to seven bipolar surface EMG channels at 2kHz from each subject. In general, we tried to use the fewest possible channels that could result in full DoF control in order to show translational potential. Thus, we opted for five channels for subjects A2, B1, B2, B3, B4 and seven channels from A1 and A3 and finally six for S1, S2 and S3. We started with using five EMG channels per subject. For the amputee subjects, we attempted to add more electrodes to improve decoding performance. Subject A2, however, had very limited surface area on the remaining forearm and so we were unable to use any additional electrodes. For the able subjects, the muscles targeted were the extensor digitorium, flexor carpi radialis, palmaris longus, flexor digitorum superficialis and flexor carpi ulnaris, located with palpation. Due to the differences in the cause of amputation (ex. Torsion vs. lacerating), remaining muscles in the forearm differed in placement from non-amputees so palpation of the stump for controllable muscle tone determined electrode placement.

EMG processing and Feature Extraction. We chose eight well-explored time-domain features to extract for both experiments 1 and 2[32,33]:

- Mean absolute value
- Zero crossing: number of time that the amplitude value of the EMG crosses zero
- Slope sign changes: number of times that the slope of the EMG amplitude changes sign
- Waveform length: cumulative length of the EMG waveform
- Log detector: $e^{\frac{1}{N}\sum_{i=1}^{N}\log(|x_i|)}$ where x_i is the EMG amplitude at time bin *i*.
- Root mean square of EMG amplitude
- Willison amplitude: number of times the difference between two EMG neighboring samples is greater than a certain threshold. In the implemented code, the threshold has been set to 0.2 times the value of the standard deviation of the global signal.
- Maximum absolute value was used only in Experiment 3.

In Experiment 1, all seven features of all channels became the inputs of the multilayer perceptron model. In experiments 1 and 2, we used a 100ms-sliding window with 50ms of overlap to calculate features, downsampled to 30Hz for the online experiments.

For a preliminary offline experiment (Supplementary Figure 1), we also calculated four autoregressive features. Before fitting the MLP, we performed both channel and feature selection so not all features were included in the network training. In channel selection, one MLP was first trained and tested for each EMG channel. The channel providing the highest estimation performance was chosen as the first optimal channel. In the second fit iteration, the previously selected channel was paired with each of the remaining channels. These pairs were then used to train and test other MLPs. Again, the pair providing the highest estimation performance was chosen as the optimal subset of two channels. This procedure was repeated until either the increase in coefficient of determination (R^2) after adding one channel was less than 0.01 or a limit of 5 channels was reached. For feature selection, the same forward selection algorithm as for channel selection was used, repeating as long as the increase in R^2 after adding one feature was greater than 0.01. For the third experiments, we used a 300ms sliding window with 30ms overlap to extract features offline. Online frequency was kept the same, no feature selection was applied nor channel selection.

Experiments in a virtual environment (Experiments 1 and 2)

Experiment 1 began with a training period lasting approximately 3 minutes. The subject watched a series of movements on a screen performed by a pair of virtual robotic hands (Modular Prosthetic Limb by Johns Hopkins University Advanced Physics laboratory). The subject was instructed to try to copy the movements on the screen with mirrored movement (imagined movement of the phantom hand in the case of amputees). Each movement was repeated three times, each with a hold period of approximately five seconds. sEMG activity from the stump of the amputation (decomposed into features) and the directed movements of the virtual hand served as training signals for the MLP. Thus, we assumed perfect tracking between the subject and the movements presented on the screen. We asked subjects to perform single finger flexions and extensions, thumb opposition, closed hand, three-finger pinch, ulnar grasp, and open hand (Figure 1c). Due to subject A2's lack of residual active muscle, we asked only this subject to perform thumb opposition, index and middle finger combined flexions and extensions, closed hand, three-finger pinch, ulnar grasp and open hand. After the training period, subjects attempted to repeat these movements in random order, using the MLP prediction output. Again, they were cued with the virtual hand movements. Each movement was repeated five times. Either the right or left hand of the virtual hand performed the desired movement, which the subjects attempted to follow, while the other virtual hand showed the MLP-decoded output. The controllable virtual hand was ipsilateral to the amputation for amputee subjects and the dominant hand for able subjects.

During shared control, Experiment 2, the MLP output controlled one virtual hand for grasping objects. Subjects used a color cue (red/green) to signal when to grasp and release each object. Each grasp or release phase lasted seven seconds. The virtual objects presented were a cylinder, a cross-shaped joint, and a thin rectangular bar in one of three different orientations per object (rotations around either the x, y or z axes) presented at random. Subjects controlled the hand with MLP predictions of four digits: thumb, index, middle and either the ring or the pinky finger for the last finger of the Allegro Hand simulation. From the virtual environment, we are able to record data from the hand's contact sensors and hence are able to assess hand-to-object contact as well as hold time. For each object, we defined required contacts for a successful trial based on the contacts that were physically attainable. For the cylinder, required contacts were proximal interphalangeal and metacarpophalangeal contacts on every digit, for the cross-joint, required contacts were distal and proximal interphalangeal contacts on every digit, and for the rectangular bar, required contacts were

the distal phalanges of the index and ring fingers and the thumb. A trial was a success if the subject was able to achieve all required contacts simultaneously.

Experimental Hardware description

The hardware for the final "physical" experiments consists of an Allegro hand mounted on the KUKA IIWA 7 robot, OptiTrack camera system and TEKSCAN pressure sensors. The *right* allegro hand consists of three fingers and a thumb, each with four degrees of freedom. The fingers have four motors, one each at the MCP, PIP and DIP joints while the fourth motor is located just under the finger base, where it is attached to the palm and controls its lateral rotation. The thumb has three motors located at the joint connecting to the palm, controlling rotations along the three axes and one motor located at the joint connecting the two phalanges. Each of the 16 motors can be operated in position control or torque control mode, the later being used in shared control approach. A set of two TEKSCAN tactile sensor GRIP system is mounted on the allegro hand to obtain contact and pressure information at the phalanges. Due to an issue with the third finger, we had to restrain its motion completely and work with the thumb and other two fingers in all our experiments.

The allegro hand is mounted on KUKA arm so that it can be moved around in space by the subject. The subject wears a set of three OptiTrack markers on the wrist, using which the position and orientation of the subject's hand can be detected by a set of 7 infrared camera. The EE of KUKA is then sent the same to move it in tandem with subject's hand. KUKA IIWA 7 robot has 7 degrees of freedom, which allows its end-effector (EE) to be moved in desired position and orientation in smooth and continuous manner. An inverse-kinematics solver decodes the EE position and orientation into the individual desired joint positions, and sends them to the KUKA arm's controller.

Protocols of the "physical" experiments (Experiment 3).

These experiments began with a training period lasting 4 and a half minutes. The subject watched a series of movements on a screen performed by the same virtual environment as experiments 1 and 2. Each movement was repeated five times, each with a hold period of approximately five seconds. sEMG activity from the forearm of the subjects (decomposed into features) and the directed movements of the virtual hand served as training signals for the MLP. Thus, we assumed perfect tracking between the subject and the movements presented on the screen. At the end of this task, the MLP was trained.

For the "box and block" task, two hard cases were placed on a table in front of the robot with a bottle of water placed on one of them. Subjects were instructed to grab a bottle of water (Badoit 1L) and move it from one box to the other. They could grasp it freely and change grip position until they felt confident enough to lift it up. A trial was considered as success if the bottle was moved from one box to the other without droppage before reaching the second box. If the subject knocked over the bottle while trying to grasp it, the experimenter put it back at initial condition and the trial was not considered as fail.

During these experiments, several metrics were used to assess the performance of the subjects:

1. Number of successful trials performed by the subject. A trial was considered as failure if the bottle fell in the gap between the two boxes.
2. Time to perform the overall task
3. Average number of contacts and the "effective normalized pressure". These two parameters were used to characterize the quality of grasping. Owing to the varying sensitivity of the sensors, pressure of each sensor data was first normalized by dividing by the maximum detected value of the respective sensors. The normalized data were used in rest of the evaluations. The average

number of contacts on each finger was computed by summing the number of contacts detected on each finger and averaged over the grasping time of each trial. Whereas, the effective normal pressure is defined as the sum of maximum normalized pressure detected on all phalanges of a finger weighed by the average contact time of the respective phalange during the grasping period of a given trial. Usually, a greater number of contacts on each finger tends to make the grasp more stable against perturbation. Further, higher pressure and duration of contact are expected to improve the grasp in a task such as block test. Therefore, it is reasonable to assume that the two metrics defined here can be used to test shared control's performance in improving the grasp.

For the manipulation task, the same bottle was placed on a table in front of the robot. Subjects were instructed to grasp and lift the bottle, then tilt their arm as if they were drinking from it. The trial was considered successful if the water flowed to the other side of the bottle (touching the bottle cap). The subject was then required to return the arm to initial position, and then hold the bottle in the air above the table for 10 seconds without any slippage. The experimenter verified that the bottle-tilt movement phase was completed within ten seconds and that the post-movement hold period also lasted 10 seconds. The MLP was retrained between the two behavioral sessions to avoid any loss of performance and the order between the two conditions (MLP only and shared control) was reversed for each subject compared to the first session.

Multilayer perceptron model. We chose to use the multilayer perceptron as the decoding method for decoding finger kinematics due to its extensive use in sEMG applications[34]. For experiment 1 and 2, we chose a three-layer network with one input layer, one hidden layer with three neurons and an output layer. The input layer is composed of the different features extracted from sEMG data and the number of nodes is dependent on the number of channels we recorded. Each of the three neurons of the hidden layer exhibit a hyperbolic tangent activation function. The output layer is the decoded output and consists of only one parameter (DoF). Hence, the full decoder incorporates as many MLP networks as desired degrees of freedom. The decoded joints in Experiment 1 were wrist pronation/supination, index and middle finger flexion/extension and ring and little fingers flexion/extension (three DoFs total). The decoded joints in Experiments 2 and 3 were metacarpal-phalangeal joint angle and interphalangeal joint angle of each digit, and thumb opposition/reposition (11 DoFs total). For more robustness, we averaged value of the interphalangeal and metacarpal-phalangeal joints per digit and considered them one DoF for all analyses.

Model training defines the weights of each node's contribution to the next layer and in an MLP, all nodes of one layer are connected to each of the nodes of the next layer by these weights. Training was accomplished by minimizing a sum-of-squares error function. A training set with input features x_n where n is the number of time lags (n = 1, …, N) and desired kinematics t_n has the error function:

$$E(w) = \frac{1}{2}\sum_{n=1}^{N} \| y(x_n, w) - t_n \|^2$$

Here, w is the array of weights of the neurons and y are the predicted kinematics using the feature input. We chose to use the Levenberg-Marquardt method for fitting the network weights due to its faster convergence time than the more typical gradient descent methods.

In order to fit the MLP weights in Experiment 1, seven movement repetitions were used for the training set, five for the testing set and three for the validation set. We used 10-fold cross-validation in Experiment 1 and 4-fold cross-validation in Experiments 2 and 3, with the training and test sets in order to determine the optimal weights for testing. In Experiment 2, each session began with a 3-minute training phase in order to record a data set of desired movements consisting of three repetitions of each movement, of which 70% of the time was used for training and 30% for validation.

We then performed cross-validation in order to choose the optimal weights for online control. The full model-training process lasted a total of less than ten minutes for all of the subjects, with exact duration depending on the number of EMG channels used. Hence, we emphasize the practical implications of such an algorithm for clinical use.

We also performed a preliminary offline experiment in which three able-bodied subjects index and middle finger combined flexion/extension, ulnar grasp/release, and wrist pronation/supination in three different arm positions: arm extended, arm flexed, and arm at rest (supported) shown in Supplementary Figure 1. Subjects performed bilateral volitional alternating movements of each DoF while we optically tracked kinematics of the hand and arm contralateral to the one from which we recorded sEMGs. The MLP decoder was then trained and we performed offline testing of decoder performance. Decoding accuracy of the testing set for one subject is plotted in Figure 2a. With impressive R2 values of 0.82, 0.79 and 0.80 for the index and middle finger flexion/extension, ring and pinky finger flexion/extension, and wrist pronation/supination respectively, the MLP is able to predict movements with high accuracy for each of the DoFs simultaneously. In particular, the decoder adeptly tracks both the sinusoidal flexions and extensions as well as sustained flexion or extension to the full range of motion of the DoFs.

For the final "physical" experiment, the architecture of the MLP was changed slightly from the first two experiments. The MLP was designed using TensorFlow's[35] premade DNN regressor class and consisted of three fully connected layers as the other experiments but in this case the hidden layer consisted of thirty neurons that exhibited a ReLU activation function (max[0,x]). The output layer is also the decoded output and consists of only one parameter (DoF). Therefore, there was again one MLP per decoded joint. In this case, joint angle values were kept independent. The loss function was the mean squared error as before. The network was trained using adaptive moment estimation (Adam). During training of experiment 3, subjects were required to perform five repetitions of each movement; four were used as the training set and one for validation. No cross-validation was needed since we could directly see the performance in real time with the robot (~test set). The full model-training process lasted approximately ten minutes for each of the three subjects.

Online Control.

Real time software for the MLP was programmed in C++ (Visual Studio 2015)) for experiment 1 and 2, which integrated input from the EMG recording systems and sent decoded joint angles to the Modular Prosthetic Limb and to the Allegro Hand simulator in Gazebo. For experiment 3 the real-time software was programmed in Python 3.6, which received the EMG signals and sent decoded joints to the real Allegro Hand. In the C++ software, matrix functions were implemented using the Armadillo class[38] and Scilab (Scilab Enterprises 2012). After fitting of the MLP, we extracted features from EMG signals in real time. Here, we use only the most recent 100ms (or 300ms in the third experiment) of EMG data for feature computation. We first normalize EMG amplitudes with means and standard deviations derived from the training data of the same channels and then made prediction updates at 33Hz (every 30ms). To obtain a smoother signal, we low-pass filtered the MLP output with a 10-frame moving average and in the third experiment, a Kalman filter was added after the moving average filter.

Shared Controller. The autonomous controller for the shared-control condition adapted from the compliant contact approach published by Sommer and Billard for the maximization of "desired contact points" with objects[23]. As soon as the hand is in contact with the object, the controller moves the fingers in directions that increase the area in contact. It stops once it has established a contact at all desired contact points. The digits are controlled in torque-mode at all times. The controller's principle is based on operational space control. That is, it projects the forces/torques in the nullspace of the contact forces. The controller can also modulate the torques in the fingers' joints to generate the

desired forces at the contact point so as to stabilize the object. For a complete mathematical description of the approach, the reader can refer to Sommer and Billard[23].

Depending on the task, different types of contact points and numbers of contacts can be defined. In our implementation, we used a Gazebo simulator of the Allegro Hand, which is a 4-digted robotic hand with simulated contact sensors on the inner, side and top surface of each digit. The hand has three phalanges per digit and joints between the phalanges can all be independently controlled in torque, for a total of 16 actuated degrees of freedom. We defined one desired contact per phalanx of each finger and two for the thumb for a total of 11 desired contacts on the simulator. When the hand is not touching any objects, a proportional-derivative (PD) controller modulates joint torques to achieve the desired joint angle targets. These targets are the angles decoded by the MLP, and streamed to the simulation over UDP. Instead of predefined preshaping as in the previous work, preshaping is left to the user. Indeed, we observed thumb opposition before finger flexion for many subjects (see Supplementary Video 2), which allowed them high grasp stability. In lieu of the drill object tested previously, we presented a thin rectangular bar along with the cylinder and cross joint part (Suppl. Fig. 3a). Each object was tested in one of three random orientations, 30 degrees tilted in either roll, pitch or yaw. This allowed exploration of the full range of object locations with respect to the hand.

In the shared control condition, the algorithm attempts to maximize contact area by applying motor torques in the direction of desired contact points. Once a digit comes in contact with an object at any location, the controller will exert joint torques on the hand in order to achieve more desired contact points with the object. The direction of these joint torques is computed as a summation of the normal vector of the contact point with the object and the direction of the desired contact towards that point (Figure 4c). If there is no contact between a digit and an object, that digit is still PD-controlled to achieve the MLP output's target angles. As for the contacts already made between the hand and the object, the shared controller exerts a predefined force, but also permits joint torques in magnitude and direction such that contact force between the desired contact and the object does not change, the contact nullspace. Thus, each digit is allowed to slide along the surface of the object to continue seeking contact with the object at "desired contacts" that have not yet been achieved. Meanwhile, the PD controller continues to compute the joint torques required to achieve MLP-dictated joint angles. The shared controller applies the vector components of these joint torques at already-achieved contacts such that the those contact forces do not change. The result is that the user is still able to move the hand over the object as desired without breaking contact. This feature made object manipulation possible.

The shared controller is designed to optimize for maximum contact between hand and object. However, if the difference in desired joint angle of the active shared controller becomes too different (defined in our case as 50 degrees total difference amongst all joints of a digit) from the decoded MLP output, the PD controller takes over again using MLP-decoded joint angles as target angles. Thus, any contact that may already exist could freely be broken.

Code availability

The MATLAB code used for data analysis and synthesis of results presented in this study are available at https://github.com/KZzizzle/0713.git. Data collection code is available from the corresponding author on reasonable request.

Data availability

The data that support the findings of this study are available within the paper and its Supplementary Information. All datasets generated for this study are available from the corresponding author upon reasonable request.

Author Contributions

K.Z. and E.F. designed and carried out Experiments 1-2, and performed analysis of data. A.B. and S.M. were responsible for planning and supervising of the work. N.S. provided code and expertise for the shared controller and contributed greatly to experimental setup. V.M. and F. A. developed the decoding algorithm for Experiment 3. V.M., F.A, S.A. performed the system integration. V.M. S.A performed all the trials for Experiment 3. E.D. aided in experimentation, G.G., G.C., and W.R. were clinical liaisons, and F.P. supervised Experiment 1. K.Z., V.M., and S.A. wrote the manuscript and designed figures. N.S., E.F., E.D., A.B., F.A* and S.M. all contributed critical feedback to the manuscript.

Acknowledgements

We wish to acknowledge Brock Wester, Francesco Tenore, and the Johns Hopkins University Applied Physics Laboratory (JHU/APL) for providing the Virtual Integration Environment (VIE), which was developed on the Defense Advanced Research Projects Agency (DARPA) Revolutionizing Prosthetics program under Contract No. N66001-10-C-4056. We would also like to thank Francesco Iberite for his assistance in conducting experiments and Alexis Devillars for the development of the Unity model of the hand.

This project was partly funded by the Swiss National Competence Center for Research (NCCR) in Robotics, by the Bertarelli Foundation, and by the European Union's Horizon 2020 research and innovation programme under Marie Skolodowska Cruie grant agreement No. 750947 (project BIREHAB).

References

1. Ziegler-Graham, K., MacKenzie, E. J., Ephraim, P. L., Travison, T. G. & Brookmeyer, R. Estimating the Prevalence of Limb Loss in the United States: 2005 to 2050. *Arch. Phys. Med. Rehabil.* **89**, 422–429 (2008).
2. Watve, S., Dodd, G., MacDonald, R. & Stoppard, E. R. Upper limb prosthetic rehabilitation. *Orthop. Trauma* **25**, 135–142 (2011).
3. Geethanjali, P. Myoelectric control of prosthetic hands: state-of-the-art review. *Med. Devices Auckl. NZ* **9**, 247 (2016).
4. Biddiss, E. & Chau, T. Upper-Limb Prosthetics: Critical Factors in Device Abandonment. *Am. J. Phys. Med. Rehabil.* **86**, (2007).
5. Biddiss, E. A. & Chau, T. T. Upper limb prosthesis use and abandonment: A survey of the last 25 years. *Prosthet. Orthot. Int.* **31**, 236–257 (2007).
6. Farina, D. *et al.* The Extraction of Neural Information from the Surface EMG for the Control of Upper-Limb Prostheses: Emerging Avenues and Challenges. *IEEE Trans. Neural Syst. Rehabil. Eng.* **22**, 797–809 (2014).
7. Hioki, M. & Kawasaki, H. Estimation of Finger Joint Angles from sEMG Using a Neural Network Including Time Delay Factor and Recurrent Structure. **2012**, (2012).
8. Malešević, N. *et al.* Decoding of individual finger movements from surface EMG signals using vector autoregressive hierarchical hidden Markov models (VARHHMM). in *2017 International Conference on Rehabilitation Robotics (ICORR)* 1518–1523 (2017). doi:10.1109/ICORR.2017.8009463
9. Tenore, F. V. G. *et al.* Decoding of Individuated Finger Movements Using Surface Electromyography. *IEEE Trans. Biomed. Eng.* **56**, 1427–1434 (2009).
10. Smith, R. J., Tenore, F., Huberdeau, D., Etienne-Cummings, R. & Thakor, N. V. Continuous decoding of finger position from surface EMG signals for the control of powered prostheses. in

2008 30th Annual International Conference of the IEEE Engineering in Medicine and Biology Society 197–200 (2008). doi:10.1109/IEMBS.2008.4649124

11. Ngeo, J. G., Tamei, T. & Shibata, T. Continuous and simultaneous estimation of finger kinematics using inputs from an EMG-to-muscle activation model. *J. NeuroEngineering Rehabil.* **11**, 122 (2014).
12. Krasoulis, A., Vijayakumar, S. & Nazarpour, K. Evaluation of regression methods for the continuous decoding of finger movement from surface EMG and accelerometry. in *2015 7th International IEEE/EMBS Conference on Neural Engineering (NER)* 631–634 (2015). doi:10.1109/NER.2015.7146702
13. Cipriani, C. *et al.* Online myoelectric control of a dexterous hand prosthesis by transradial amputees. *IEEE Trans. Neural Syst. Rehabil. Eng.* **19**, 260–270 (2011).
14. Jiang, N., Dosen, S., Muller, K. R. & Farina, D. Myoelectric Control of Artificial Limbs—Is There a Need to Change Focus? [In the Spotlight]. *IEEE Signal Process. Mag.* **29**, 152–150 (2012).
15. Kim, H. K. *et al.* Continuous shared control for stabilizing reaching and grasping with brain-machine interfaces. *IEEE Trans. Biomed. Eng.* **53**, 1164–1173 (2006).
16. Iturrate, I., Montesano, L. & Minguez, J. Shared-control brain-computer interface for a two dimensional reaching task using EEG error-related potentials. in *2013 35th Annual International Conference of the IEEE Engineering in Medicine and Biology Society (EMBC)* 5258–5262 (2013). doi:10.1109/EMBC.2013.6610735
17. Chen, X. *et al.* A shared control policy for center-out movement decoding in motor Brain-machine Interface. *3rd IFAC Conf. Intell. Control Autom. Sci. ICONS 2013* **46**, 345–348 (2013).
18. Ciancio, A. L. *et al.* Control of Prosthetic Hands via the Peripheral Nervous System. *Front. Neurosci.* **10**, 116 (2016).

19. Došen, S. *et al.* Cognitive vision system for control of dexterous prosthetic hands: Experimental evaluation. *J. NeuroEngineering Rehabil.* **7**, 42–42 (2010).
20. Light, C. M., Chappell, P. H., Hudgins, B. & Engelhart, K. Intelligent multifunction myoelectric control of hand prostheses. *J. Med. Eng. Technol.* **26**, 139–146 (2002).
21. Tura, A., Lamberti, C., Davalli, A. & Sacchetti, R. Experimental development of a sensory control system for an upper limb myoelectric prosthesis with cosmetic covering. *J. Rehabil. Res. Dev.* **35**, 14–26 (1998).
22. Fani, S. *et al.* Assessment of Myoelectric Controller Performance and Kinematic Behavior of a Novel Soft Synergy-Inspired Robotic Hand for Prosthetic Applications. *Front. Neurorobotics* **10**, 11 (2016).
23. Sommer, N. & Billard, A. Multi-contact haptic exploration and grasping with tactile sensors. *Robot. Auton. Syst.* **85**, 48–61 (2016).
24. Celadon, N., Došen, S., Binder, I., Ariano, P. & Farina, D. Proportional estimation of finger movements from high-density surface electromyography. *J. NeuroEngineering Rehabil.* **13**, 73 (2016).
25. Segil, J. L., Controzzi, M., Weir, R. F. ff & Cipriani, C. Comparative study of state-of-the-art myoelectric controllers for multigrasp prosthetic hands. *J. Rehabil. Res. Dev.* **51**, 1439–1454 (2014).
26. Mathiowetz, V., Volland, G., Kashman, N. & Weber, K. Adult norms for the Box and Block Test of manual dexterity. *Am. J. Occup. Ther.* **39**, 386–391 (1985).
27. Park, E. & Meek, S. G. Fatigue compensation of the electromyographic signal for prosthetic control and force estimation. *IEEE Trans. Biomed. Eng.* **40**, 1019–1023 (1993).
28. Tkach, D., Huang, H. & Kuiken, T. A. Study of stability of time-domain features for electromyographic pattern recognition. *J. NeuroEngineering Rehabil.* **7**, 21 (2010).

29. Asghari Oskoei, M. & Hu, H. Myoelectric control systems—A survey. *Biomed. Signal Process. Control* **2**, 275–294 (2007).
30. Micera, S., Carpaneto, J. & Raspopovic, S. Control of Hand Prostheses Using Peripheral Information. *IEEE Rev. Biomed. Eng.* **3**, 48–68 (2010).
31. Wan, B. *et al.* Study on fatigue feature from forearm SEMG signal based on wavelet analysis. in *2010 IEEE International Conference on Robotics and Biomimetics* 1229–1232 (2010). doi:10.1109/ROBIO.2010.5723504
32. Zardoshti-Kermani, M., Wheeler, B. C., Badie, K. & Hashemi, R. M. EMG feature evaluation for movement control of upper extremity prostheses. *IEEE Trans. Rehabil. Eng.* **3**, 324–333 (1995).
33. Phinyomark, A., Phukpattaranont, P. & Limsakul, C. Feature reduction and selection for EMG signal classification. *Expert Syst. Appl.* **39**, 7420–7431 (2012).
34. Chu, J. U., Moon, I. & Mun, M. S. A Real-Time EMG Pattern Recognition System Based on Linear-Nonlinear Feature Projection for a Multifunction Myoelectric Hand. *IEEE Trans. Biomed. Eng.* **53**, 2232–2239 (2006).
35. Abadi, M. *et al.* Tensorflow: A system for large-scale machine learning. in 265–283 (2016).